Geomorphological monitoring of erosion on restored slopes through the integration of drones, GIS, and LiDAR

Mónica López Moncada[1,2,3], Joan-Cristian Padró[1,4], Vicenç Carabassa[5], Paulo Escandón-Panchana[6,7], Andrés Velastegui-Montoya[2,3]

[1] Departamento de Geografía, Universitat Autònoma de Barcelona (UAB), Bellaterra, Catalonia, Spain – joancristian.padro@uab.cat
[2] Faculty of Engineering in Earth Sciences, ESPOL Polytechnic University, Guayaquil, Ecuador – mirlopez@espol.edu.ec
[3] Laboratory of Geoinformation and Remote Sensing, Faculty of Engineering in Earth Sciences, ESPOL Polytechnic University, Guayaquil, Ecuador – dvelaste@espol.edu.ec
[4] Institut Cartogràfic i Geològic de Catalunya (ICGC), Parc de Montjuïc, E08038 Barcelona, Spain
[5] CREAF, Universitat Autònoma de Barcelona (UAB), Bellaterra, Catalonia, Spain – v.carabassa@creaf.uab.cat
[6] Departamento de Ingeniería Cartográfica y Topografía, Universidad Politécnica de Madrid (UPM), Madrid, Spain – pc.escandon@alumnos.upm.es
[7] Escuela de Ciencias Ambientales, Universidad Espíritu Santo, Samborondón, 0901952, Ecuador

Keywords: Mine Restoration, Slope Erosion, Geospatial Analysis, Drone Photogrammetry, DEM, LiDAR.

Abstract

Mining is a strategic driver of economic development, yet it generates substantial impacts on landscape structure, soil integrity, and water systems. During ecological restoration, slope erosion remains a critical challenge for ensuring long-term geomorphological stability and ecosystem recovery. This study evaluates erosion dynamics on restored mining slopes by integrating Geographic Information Systems (GIS) and Unmanned Aerial Systems (UAS) for high-resolution terrain monitoring and quantification of soil loss. Research was conducted at the Lázaro quarry (Tarragona, Spain) using a fixed-wing UAS equipped with a multispectral camera to produce detailed orthophotos and Digital Elevation Models (DEMs), which were compared with historical LiDAR data. Height Difference Models (HDMs) and volumetric calculations were applied to quantify erosion and deposition. Statistical assessment included descriptive indicators, error metrics (ME, MAE, RMSE), distribution parameters (median, IQR, skewness), and spatial autocorrelation (Moran’s I). Three modelling approaches were developed and compared: a ridge-derived DEM (DEMp), a filtered DEM (DEMf), and a LiDAR-based DEM (DEMl). Their performance was evaluated in terms of accuracy, spatial resolution, and capacity to represent erosional microtopography. Results indicate that DEMp provides the most reliable volume estimates and best preserves pre-erosion morphology. In contrast, DEMf smooths surface detail, whereas DEMl provides an overview representation due to its lower spatial resolution. Overall, the integration of UAS photogrammetry and geospatial analysis proves effective for monitoring restored slopes, supporting precise erosion quantification and improved environmental management toward long-term landscape stability.

1. Introduction

Mining is a strategic activity for global economic development, providing essential raw materials and energy resources that support modern industry and technology (Ren et al., 2019). However, mining operations have a significant impact on the landscape, soil, and water resources, especially in open-pit mining areas (Guedes et al., 2021). During the restoration phase, one of the primary challenges is controlling surface erosion and ensuring the geomorphological stability of rehabilitated slopes, which are decisive factors for the environmental sustainability of a site (Carabassa et al., 2020).

Monitoring erosion processes on slopes requires high-resolution topographic data to identify microforms, volumetric changes, and drainage patterns (Lindsay and Seibert, 2013; Sabzevari and Talebi, 2019). However, conventional topographic survey techniques are expensive and have limited spatial coverage, making the continuous monitoring of large or hard-to-reach areas difficult (Azizian, 2019). In this context, remote sensing (RS) using Unmanned Aerial Systems (UAS) has been established as an efficient and cost-effective alternative, capable of generating Digital Elevation Models (DEM) and orthophotos with centimetre resolution (Esposito et al., 2017).

The integration of UAS-derived products with LiDAR data and Geographic Information Systems (GIS) tools has shown high potential for analysing terrain erosion dynamics (Alexiou et al., 2024; Đomlija et al., 2019; Escandón-Panchana et al., 2025). The use of UAS in mining has shown remarkable potential to generate accurate Digital Elevation Models (DEM) for morphometric analysis, three-dimensional reconstruction, geological risk assessment, and environmental monitoring (Padró et al., 2019a, 2019b). Likewise, the integration of DEMs derived from digital photogrammetry and laser altimetry has enabled the quantification of topographic changes associated with erosion processes with high reliability (Eltner et al., 2013; Evans and Lindsay, 2010). However, most previous studies have focused on agricultural or watershed environments, and the application of these approaches in mining restoration areas remains limited. Furthermore, few studies systematically compare the accuracy and representativeness of DEMs generated by drone photogrammetry versus those obtained using LiDAR sensors.

Faced with this gap, this study aims to estimate erosion on restored slopes of the Lázaro quarry (Tarragona, Spain) by integrating UAS data, GIS analysis and Height Difference Models (HDMs) to quantify topographic variations and analyse the consistency between different photogrammetric and LiDAR modelling approaches. This research presents a replicable, cost-

This contribution has been peer-reviewed.
https://doi.org/10.5194/isprs-archives-XLIX-B2-2026-1059-2026 |

effective methodology for geomorphological monitoring in restored mining areas, thereby contributing to the development of spatial analysis tools for environmental management and to the assessment of the effectiveness of land restoration processes.

2. Study area

The Area of Interest (AOI) corresponds to the Lázaro quarry, a mining operation located in the municipality of El Vendrell (Tarragona, northeast Spain), with an approximate area of 60 ha and a perimeter of 3.7 km (Figure 1) (Carabassa et al., 2021). This quarry exemplifies the characteristic extractive activity in carbonate materials within the Catalan coastal sector, where post-exploitation geomorphological dynamics necessitate the implementation of restoration strategies and environmental monitoring (Solé et al., 2023).

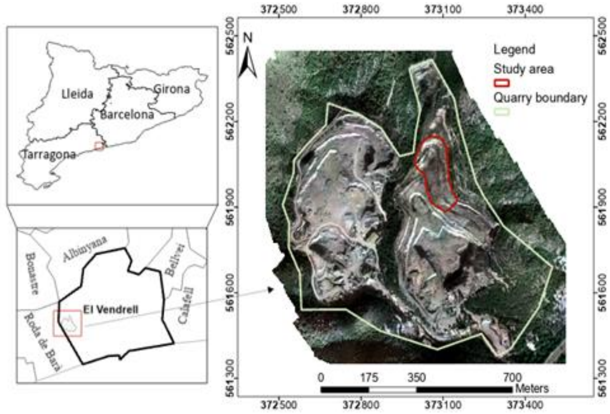

Figure 1. Location of the study area: Lázaro Quarry, Tarragona, Spain.

From a geological perspective, the AOI is primarily composed of two lithological units. In the northern zone, limestone, dolomitic limestone and marlystone from the Lower Cretaceous predominate, while in the southern zone, calcarenites from the Miocene outcrop (Sendrós et al., 2023). These carbonate formations have a relatively massive and fractured structure, which favours surface instability and the development of erosive processes when the soil cover is altered (Padró et al., 2022). Under natural conditions, Tertiary materials are relatively resistant to erosion; however, anthropogenic interventions, such as mining and clearing techniques, have intensified gully formation and soil loss due to concentrated runoff, a common phenomenon on Mediterranean quarry slopes (Martín-Velázquez et al., 2022).

The average thickness of materials with commercial value reaches approximately 106 m, corresponding to compact limestone rocks used in the production of aggregates and cement (INECO, 2017). This study focuses on a 23,189.66 m² subarea located northeast of the quarry, where restoration work was carried out in the early 2010s. The intervention consisted of constructing high-slope slopes (>30°) using a slope-berm model. However, the lower slopes, composed mainly of waste materials without stabilisation or soil amendments, exhibit low vegetation cover and high susceptibility to erosion, compromising the geomorphological stability and ecological functionality of the restored area.

3. Methodology

The methodology is structured into six integrated phases that combine photogrammetric techniques, geospatial analysis, and digital terrain modelling for evaluating erosion dynamics on restored slopes (Figure 2). This approach generated, processed, and compared high-resolution DEMs from UAS and remote sensing data, ensuring accurate detection of morphological changes.

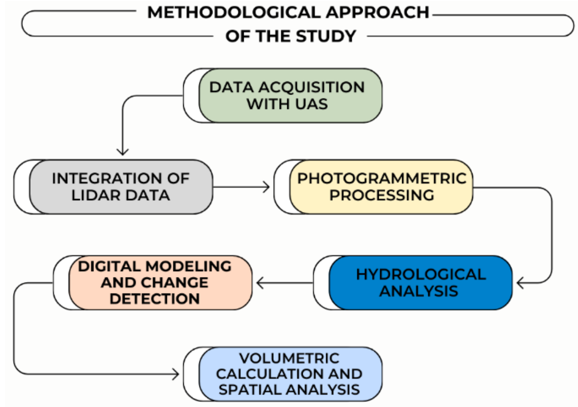

Figure 2. Methodological approach of the study.

3.1 Phase I: Data acquisition with UAS

The aerial survey was conducted on January 8, 2020, using an Atmos-7 fixed-wing drone (CATUAV), with a 70-minute endurance and a 5-km telemetry range, to ensure complete coverage of the restored slopes. The flight was conducted at an altitude of 120 meters above ground, under stable meteorological conditions. A MicaSense RedEdge-M multispectral camera was used for data capture, simultaneously recording five spectral bands (blue, green, red, red edge, and near-infrared), allowing characterisation of vegetation cover and soil surface conditions (Xiao et al., 2022).

The georeferencing was based on 10 Ground Control Points (GCP) and three validation points, obtained from orthophotos and DEMs from the Cartographic and Geological Institute of Catalonia (ICGC), achieving an accuracy of $RMSE_x = 0.11$ m, $RMSE_y = 0.19$ m and $RMSE_z = 0.45$ m. This configuration has demonstrated high reliability in precision geomorphological studies (Clay et al., 2022).

3.2 Phase 2: LiDAR Data Integration

LiDAR data from 2016 were incorporated (ICGC, 2020), with an average point density of 1 point/m² and a root-mean-square error of 0.06 m. This data was classified into 17 categories according to the ASPRS standard. UAS-LiDAR data integration improves the detection of erosional microforms and reduces uncertainty in temporal surface comparison (Renette et al., 2024).

3.3 Phase 3: Photogrammetric processing

The acquired images were processed using Structure from Motion (SfM) techniques to generate the 3D point cloud, the multispectral orthophoto and the high-resolution DEM (Pell et al., 2022). Photogrammetric processing included image alignment, camera calibration, dense reconstruction, and mosaicking. This procedure was performed using MiraMon 8.2

(Pons, 2004) and Agisoft Metashape, adhering to best practices in high-precision photogrammetry (Finn et al., 2023).

3.4 Phase 4: Hydrological analysis

From the DEM, flow direction and accumulation were calculated using the D8 algorithm to identify drainage networks and watersheds (Xie et al., 2022). High accumulation values indicated concentrated flows that guided the delimitation of active ridges and slopes. Subsequently, a hierarchical drainage network was generated, and a subcloud of 3D points corresponding to the upper sectors of the slopes was delineated, excluding the points from the valleys (Wang and Koo, 2021).

3.5 Phase 5: Digital modeling and change detection

Three reference models were built to estimate erosion: DEMp (ridge-derived DEM): Constructed from the ridge point cloud using a TIN (Triangular Irregular Network) model, subsequently converted to a raster, representing the pre-erosion topography; DEMf (filtered DEM): Obtained using a median morphological filter on the current DEM to eliminate depressions and smooth the surface; DEMl (lidar DEM): Generated from the 2016 dataset, cleaned and reclassified.

From these models, Height Difference Models (HDMs) were developed to quantify the vertical changes resulting from erosion and deposition processes, as described by the HDM equation (Xinwei et al., 2023). This approach allowed the generation of HDMp, HDMf, and HDMl products for comparison between photogrammetric and LiDAR approaches.

$$HDM = DEMcurrent - DEMprevious \qquad (1)$$

3.6 Phase 6: Volumetric calculation and spatial analysis

The volumes of erosion and deposition were estimated using the Geomorphic Change Detection tool (GCD 7.4), accounting for the spatial resolution (0.10 m) and a minimum detection threshold based on the vertical error (Riverscapes Consortium, 2025). Negative values represented loss of material (erosion), and positive values represented accumulation. Finally, the results were spatialized and validated using GIS analysis in ArcGIS Pro, integrating topographic layers and slope maps.

This methodological approach enabled the precise quantification of geomorphological variations in restored slopes and the evaluation of the effectiveness of mining rehabilitation actions, demonstrating the utility of UAS-LiDAR-GIS integration for monitoring erosion processes in Mediterranean environments.

4. Results

4.1 Ridge detection

The automated ridge detection, derived from the proposed methodological flow, showed a high correspondence with the visual interpretation of the digital shadow model. Figure 3 shows that the crests of the slopes coincide with the highest elevations and the axes of the dominant streams. The shadow model reveals linear artefacts resulting from the DEM triangulation process, though they do not significantly affect the delineation of the prominent ridges.

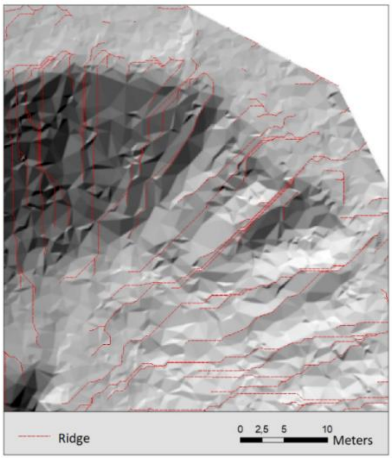

Figure 3. Schematic of ridges derived from the original DEM in a representative subarea of the study area.

4.2 Simulated digital elevation models and Statistical comparison

Figure 4 shows the DEMs generated for the pre-erosion scenario, as described in Section 3.5. The models exhibit elevation differences of ±1.00 m at the maximum elevations and ±10.00 m at the minimum elevations, reflecting the ability of each approach (ridge detection, filtering, and LiDAR data) to represent the original morphology.

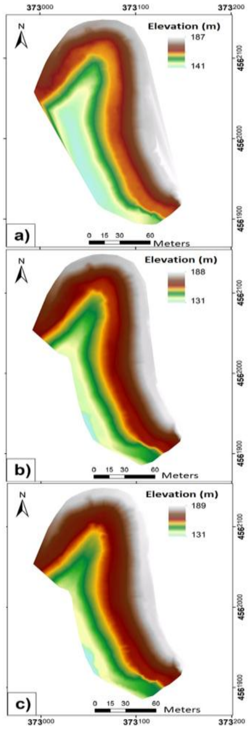

Figure 4. Pre-erosion digital terrain models: a) DEMp derived from ridges, b) DEMf obtained by filtering, c) DEMl generated from 2016 LiDAR data.

The descriptive statistics for the three Digital Elevation Models, summarised in Table 1, reveal high overall consistency in elevation ranges, although systematic differences are evident. DEMp presents a mean elevation of 165.69 m (SD = 12.23 m), while DEMf shows a slightly lower mean (164.66 m) and reduced dispersion (SD = 11.76 m), reflecting the filtering process's smoothing effect. In contrast, DEMl exhibits the highest mean elevation (167.33 m) and the largest elevation range, suggesting a vertical offset relative to the photogrammetric models. These results indicate that while DEMf and DEMl tend toward terrain generalisation, DEMp preserves morphological structure consistent with ridge-based reconstruction.

Model	Min (m)	Max (m)	Mean (m)	SD
DEMp	140.85	188.74	165.69	12.23
DEMf	131.36	187.33	164.66	11.76
DEMl	131.37	189.05	167.33	12.36

Table 1. Statistical parameters of the DEMs.

The vertical accuracy and systematic deviations of the evaluated models were assessed relative to the current UAS-derived DEM using stable ridge sectors as reference surfaces. The photogrammetric models (DEMp and DEMf) exhibit centimetric RMSE values (< 0.21 m), indicating high internal geometric consistency and low random noise levels (Table 2). DEMp presents a slight negative mean error (ME = −0.04 m), suggesting minor underestimation of elevation, while DEMf shows near-zero bias (ME = 0.02 m), reflecting the smoothing effect of median filtering.

In contrast, DEMl shows substantially larger deviations (ME ≈ −2.59 m; RMSE ≈ 2.88 m). These discrepancies reflect the combined influence of temporal mismatch (2016–2020), lower spatial resolution (1 pt/m²), and potential vertical datum inconsistencies. Therefore, error metrics for DEMl should be interpreted as resulting from both geometric misalignment and genuine topographic change, rather than solely from sensor inaccuracy.

Model	ME	MAE	RMS	ME
DEMp	-0.04	0.11	0.21	-0.04
DEMf	0.02	0.11	0.19	0.02
DEMl	-2.59	2.61	2.87	-2.59

Table 2. Error metrics and model performance.

4.3 Height Difference Model (HDM)

Figure 5 shows the MDAs between the current DEM (drone) and the pre-erosion models. These products form the basis for estimating slope volume loss due to erosion.

In the DEMp model, the differences are concentrated between 1.60 m and -0.30 m, with an eroded area of 2434.84 m² (See Figure 5a). The red areas represent areas with greater erosion, while the green areas indicate material accumulation.

The HDMf model, on the other hand, presents a range between 0.30 m and -0.15 m, covering a smaller area of 494.40 m² (See Figure 5b). However, this model fails to highlight the main gullies clearly.
For its part, the HDMl model, compared with the 2016 LiDAR data, shows discrepancies of up to -6.00 m (Figure 5c), attributable to the difference in resolution and acquisition period. Table 3 shows the vertical variability among the three HDMs. HDMf has the lowest standard deviation, indicating greater homogeneity and less topographic noise than the other models. In contrast, HDMp and HDMl exhibit greater altimetric dispersion, attributable to differences in reconstruction method and LiDAR data spatial resolution.

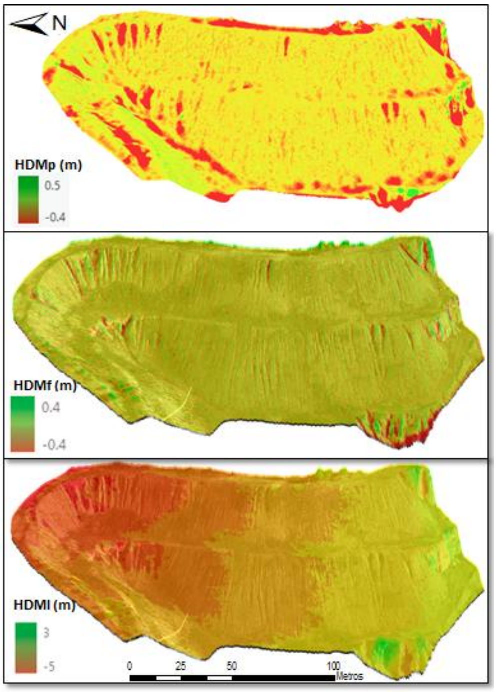

Figure 5. 3D view of the Height Difference Model between the DEMcurrent and: a) DEMp, b) DEMf, c) DEMl.

Model	Min (m)	Max (m)	Mean (m)	SD
HDMp	-3.68	1.48	-0.10	0.31
HDMf	-2.75	2.06	0.00	0.10
HDMl	-5.92	4.25	-2.65	1.27

Table 3. Statistical parameters of the HDMs.

The distributional statistics for the Height Difference Models (HDMs), summarised in Table 4, reveal distinct geomorphological behaviours across the study area. HDMp exhibits a median near zero (–0.03 m) and a moderate interquartile range (IQR = 0.16 m), indicating controlled variability that preserves subtle erosion signals. The strong negative skewness (–2.59) in this model confirms the predominance of erosional processes over deposition. In contrast, HDMf shows the lowest IQR (0.008 m), indicating excessive smoothing and reduced sensitivity to microtopographic variations, likely reflecting stabilised sectors with no active operations.

Conversely, HDMl shows the highest dispersion (IQR = 1.09 m) and a markedly negative median (–3.76 m). These metrics, combined with a near-zero skewness (0.18), suggest a relatively uniform and intense topographic lowering associated with extractive activity. While the magnitude of material removal dominates the HDMl dataset, the statistical profile of HDMp offers the most balanced representation between robust error control and geomorphological realism.

Model	Median	IQR	SKEWNESS
HDMp	-0.03	0.16	-2.59
HDMf	-0.001	0.008	1.01
HDMl	-3.76	1.09	0.18

Table 4. Statistical parameters of the HDMs.

The spatial structure and vertical accuracy of the Height Difference Models (HDMp, HDMf, and HDMl) were evaluated through Moran's I spatial autocorrelation and standard error metrics (Table 5). All models exhibited near-perfect positive

https://doi.org/10.5194/isprs-archives-XLIX-B2-2026-1059-2026 | © Author(s) 2026. CC BY 4.0 License.

spatial autocorrelation, with Moran’s I values ranging from 0.98 to 0.99 and exceptionally high Z-scores (>2130, $p < 0.001$). These results confirm that the detected elevation changes are not stochastic noise but are organised into statistically significant geographic clusters.

Model	I	Z-score	p-value
HDMp	0.98	2130.53	0.001
HDMf	0.98	2151.16	0.001
HDMl	0.99	2177.64	0.001

Table 5. Spatial autocorrelation Moran’s of the HDMs.

Although Moran’s I values approach unity (0.98–0.99), such high spatial autocorrelation partly reflects the inherent spatial continuity of topographic surfaces. Therefore, Moran’s I should be interpreted as confirmation of structured spatial patterns rather than as an independent indicator of geomorphological validity. The geomorphic plausibility of clustering must be assessed in conjunction with visual inspection and statistical dispersion metrics.

Additionally, Figure 6 compares topographic profiles along a representative transect on restored slopes. In the profile of the ridge-derived model (Figure 6b), a continuous and coherent reconstruction of the original relief is visible, preserving local altimetric changes without introducing irregularities. In contrast, the filtered model (Figure 6c) excessively smooths the microforms, reducing the expression of gullies and overestimating the terrain's regularity. The LiDAR-based model (Figure 6d) underestimates elevations, suggesting vertical discrepancies due to lower spatial resolution and the time difference between the LiDAR data and the drone flight.

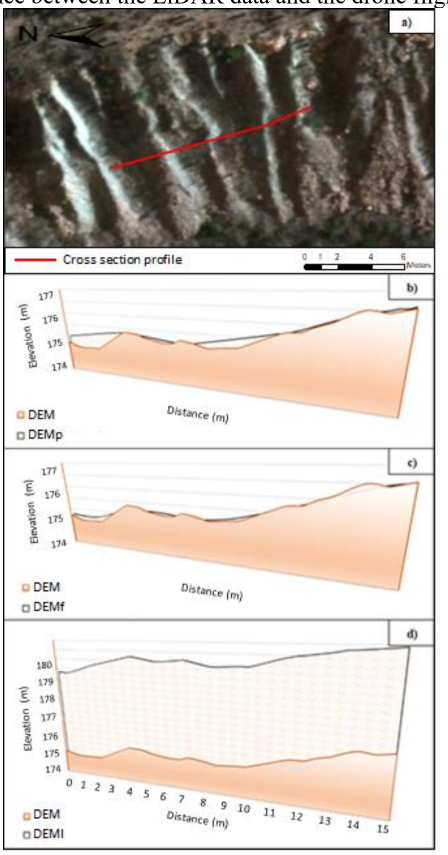

Figure 6. Comparison of topographic profiles along the representative transect on the restored slopes: a) location of the transect on the UAS orthoimage, b) profile of the DEMp, c) profile of the DEMf, and d) profile of the DEMl.

4.4 Volumetric estimation

The global volumetric estimate (See Table 6) shows that the DMEp records 75.31% erosion and 24.69% deposition, the DEMf 65.21% and 34.79% respectively, and the DEMl 99.63% erosion, suggesting an overestimation influenced by the time difference and the resolution of the LIDAR data.

Model	Erosion (m^3)	Deposition (m^3)	Net volumen (m^3)
DEMp	2418.75	703.02	-1625.73
DEMf	958.84	511.55	-447.29
DEMl	63922.77	239.58	-63683.09

Table 6. Global volumetric estimates.

When a threshold of 0.10 m is applied (Table 7), topographic noise is reduced, improving the delimitation of affected areas.

Volume	DEMp	DEMf	DEMl
Total erosion volume (m^3)	2169.73	500.41	63920.74
Total deposition volume (m^3)	407.56	233.85	238.42
Net volume difference (m^3)	-1762.18	-266.56	-63682.32

Table 7. Volumetric estimates with a threshold of 0.10 m.

The results (Table 8, threshold of 0.64 m) show that the magnitude of the change decreases significantly, demonstrating the high sensitivity of the estimated volume to the vertical uncertainty of the model.

Volume	DEMp	DEMf
Total erosion volume (m^3)	1010.95	48.95
Total deposition volume (m^3)	23.75	26.04
Net volume difference (m^3)	-987.20	-22.91

Table 8. Volumetric estimates with a threshold of 0.64 m.

Generally, the 0.10 m threshold provides a more realistic delineation of morphological changes, whereas the 0.64 m threshold tends to underestimate minor topographic variations.

5. Discussion

The integration framework proposed in this study allows not only the comparison of independently generated DEMs but also the systematic evaluation of their geometric consistency and geomorphological plausibility prior to change detection analysis. This distinction is essential, as volumetric estimates derived from multi-source DEMs are highly sensitive to vertical misalignment and differences in spatial resolution.

The performance of the DEMp ridge-detection model demonstrates its potential to reconstruct pre-erosive surfaces in a manner consistent with the actual topography. The topographic profiles obtained (Figure 6) corroborate that the ridge-derived model (DEMp) reproduces the pre-erosive morphology with greater coherence, validating its suitability compared to filtering-based or LiDAR-based approaches. The statistical comparison of the DEMs reveals subtle but meaningful differences in elevation structure. Although the three models exhibit comparable elevation ranges, DEMl shows a higher mean elevation and greater dispersion, suggesting a systematic vertical offset relative to the photogrammetric models. In contrast, DEMp maintains a stable altimetric distribution consistent with ridge-controlled reconstruction. The reduced standard deviation in DEMf confirms the smoothing effect of median filtering, which attenuates local variability reported by Laso et al. (2019).

In comparison, the DEMf model tends to smooth out local microvariations, reducing its ability to represent erosional microforms. This behaviour coincides with that reported by Laso et al. (2019), who observed that median filters applied to photogrammetric DEMs can lead to a loss of topographic detail. On the other hand, error metrics further clarify model performance. The photogrammetric models (DEMp and DEMf) show centimetric RMSE values (<0.21 m), confirming high geometric reliability for erosion detection. DEMp exhibits a slight negative mean error, suggesting minimal underestimation of vertical differences, while DEMf presents near-zero bias but slightly reduced geomorphological sensitivity. Conversely, DEMl displays a strong systematic bias (ME ≈ −2.59 m) and an RMSE exceeding 2.8 m, more than an order of magnitude higher than that of UAS-derived models. This discrepancy reflects the combined influence of temporal mismatch, lower spatial resolution, and potential vertical datum inconsistencies. These findings align with those of Cucci et al. (2017), who emphasised that volumetric accuracy strongly depends on sensor resolution and calibration quality.

The distributional analysis of the Height Difference Models provides additional insight into geomorphological realism. HDMp presents a median close to zero and a moderate interquartile range, indicating controlled variability while preserving erosion signals. Its pronounced negative skewness confirms the dominance of erosional processes over depositional ones. In contrast, HDMf exhibits an extremely low IQR, evidencing excessive smoothing and loss of microtopographic expression. HDMl shows the largest dispersion and a strongly negative median, reinforcing the presence of systematic vertical bias rather than purely geomorphic change. These results demonstrate that DEMp achieves a more balanced representation between statistical stability and morphological fidelity.

Spatial autocorrelation analysis strengthens this interpretation. All models exhibit extremely high and statistically significant Moran’s I values (>0.98), confirming that elevation differences are strongly spatially clustered rather than randomly distributed. However, the near-unity Moran’s I observed in HDMl suggests large-scale structured bias, likely reflecting vertical offset patterns across the study area rather than true geomorphological processes. In contrast, HDMp shows strong, yet geomorphologically coherent, clustering aligned with mapped gullies and drainage pathways. This distinction is critical, as high spatial autocorrelation alone does not guarantee geomorphic validity; it must be interpreted in light of error structure and terrain logic.

Furthermore, the sensitivity of volumetric estimates to the detection threshold highlights the importance of establishing appropriate values to minimise topographic noise without compromising morphological detail. In this study, a threshold of ±0.10 m was found to provide an optimal balance between geometric realism and statistical stability of the calculations, in agreement with the proposal by Cucci et al. (2017). This finding confirms that statistical validation of DEM accuracy must precede geomorphic interpretation, particularly in high-resolution erosion monitoring.

Erosion on restored slopes is one of the primary challenges in environmental management of mining areas, due to its direct impact on terrain stability, soil loss, and the sustainability of rehabilitation measures. In this context, the integration of UAS, GIS, and LiDAR data has enabled detailed characterisation of geomorphological processes, offering more precise and accessible alternatives to traditional topographic methods. The proposed methodology allows for the accurate characterisation of the morphological evolution of post-exploitation surfaces, even in contexts with limited historical information. This methodological contribution is especially relevant for strengthening mining restoration strategies and long-term geomorphological monitoring programs in Mediterranean environments.

6. Conclusions

The application of UAS enabled the generation of high-resolution digital models (<0.10 m) capable of identifying erosive microprocesses that are not detectable by conventional LiDAR sensors. This precision improves the understanding of geomorphological dynamics on mining slopes and provides valuable tools for planning environmental restorations.

The ridge-detection-based model (DEMp) showed the highest morphological and volumetric coherence among the models derived from filtering (DEMf) and lidar data (DEMl). In this sense, the methodology constitutes a viable alternative for rapid characterisation of erosion and evaluation of stability in post-exploitation slopes, thereby strengthening the technical management of restorations.

The sensitivity analysis further demonstrates that volumetric estimates are highly dependent on the selected vertical detection threshold. A ±0.10 m threshold provides an optimal compromise between noise reduction and preservation of geomorphological signal, whereas higher thresholds substantially underestimate erosional volumes. This highlights the need to incorporate statistical error diagnostics before geomorphic interpretation in DEM-based change-detection studies.

Future research recommends incorporating direct measurements and high-precision topographic points, and exploring the integration of multitemporal data and machine learning techniques to improve the detection and prediction of erosion evolution in mine restoration scenarios.

Overall, the integrated UAS–LiDAR–GIS approach provides a replicable and statistically validated methodology for erosion monitoring in restored mining environments, contributing to more reliable stability assessment and long-term restoration management.

7. References

Alexiou, S., Papanikolaou, I., Schneiderwind, S., Kehrle, V., Reicherter, K., 2024. Monitoring and Quantifying Soil Erosion and Sedimentation Rates in Centimeter Accuracy Using UAV-Photogrammetry, GNSS, and t-LiDAR in a Post-Fire Setting. Remote Sens. (Basel). 16, 802. https://doi.org/10.3390/rs16050802

Azizian, A., 2019. The Effects of Topographic Map Scale and Costs of Land Surveying on Geometric Model and Flood Inundation Mapping. Water Resources Management 33, 1315–1333. https://doi.org/10.1007/s11269-019-2202-y

Carabassa, V., Montero, P., Alcañiz, J.M., Padró, J.-C., 2021. Soil Erosion Monitoring in Quarry Restoration Using Drones. Minerals 11, 949. https://doi.org/10.3390/min11090949

Carabassa, V., Montero, P., Crespo, M., Padró, J.-C., Pons, X., Balagué, J., Brotons, L., Alcañiz, J.M., 2020. Unmanned aerial system protocol for quarry restoration and mineral extraction monitoring. J. Environ. Manage. 270, 110717. https://doi.org/10.1016/j.jenvman.2020.110717

Clay, E.R., Lee, K.S., Tan, S., Truong, L.N.H., Mora, O.E., Cheng, W., 2022. Assessing the accuracy of georeferenced point clouds from uas imagery. The International Archives of the Photogrammetry, Remote Sensing and Spatial Information Sciences XLVI-M-2–2022, 59–64. https://doi.org/10.5194/isprs-archives-XLVI-M-2-2022-59-2022

Cucci, D.A., Rehak, M., Skaloud, J., 2017. Bundle adjustment with raw inertial observations in UAV applications. ISPRS Journal of Photogrammetry and Remote Sensing 130, 1–12. https://doi.org/10.1016/j.isprsjprs.2017.05.008

Đomlija, P., Bernat Gazibara, S., Arbanas, Ž., Mihalić Arbanas, S., 2019. Identification and Mapping of Soil Erosion Processes Using the Visual Interpretation of LiDAR Imagery. ISPRS Int. J. Geoinf. 8, 438. https://doi.org/10.3390/ijgi8100438

Eltner, A., Mulsow, C., Maas, H.-G., 2013. Quantitative Measurement of Soil Erosion from TLS and UAV Data. The International Archives of the Photogrammetry, Remote Sensing and Spatial Information Sciences XL-1/W2, 119–124. https://doi.org/10.5194/isprsarchives-XL-1-W2-119-2013

Escandón-Panchana, P., Velastegui-Montoya, A., Pico-Saltos, R., Martínez-Cuevas, S., 2025. Applications of geomatics in multidisciplinary knowledge fields. A review for decision-makers. Discover Applied Sciences 7, 1409. https://doi.org/10.1007/s42452-025-07928-9

Esposito, G., Mastrorocco, G., Salvini, R., Oliveti, M., Starita, P., 2017. Application of UAV photogrammetry for the multi-temporal estimation of surface extent and volumetric excavation in the Sa Pigada Bianca open-pit mine, Sardinia, Italy. Environ. Earth Sci. 76, 103. https://doi.org/10.1007/s12665-017-6409-z

Evans, M., Lindsay, J., 2010. High resolution quantification of gully erosion in upland peatlands at the landscape scale. Earth Surf. Process. Landf. 35, 876–886. https://doi.org/10.1002/esp.1918

Finn, A., Peters, S., Kumar, P., O'Hehir, J., 2023. Automated Georectification, Mosaicking and 3D Point Cloud Generation Using UAV-Based Hyperspectral Imagery Observed by Line Scanner Imaging Sensors. Remote Sens. (Basel). 15, 4624. https://doi.org/10.3390/rs15184624

Guedes, R.S., Ramos, S.J., Gastauer, M., Júnior, C.F.C., Martins, G.C., da Rocha Nascimento Júnior, W., de Souza-Filho, P.W.M., Siqueira, J.O., 2021. Challenges and potential approaches for soil recovery in iron open pit mines and waste piles. Environ. Earth Sci. 80, 640. https://doi.org/10.1007/s12665-021-09926-7

ICGC, 2020. Topografía Territorial [WWW Document]. https://visors.icgc.cat/appdownloads/index.html.

INECO, 2017. Geología y Procedencia de Materiales.

Laso, F.J., Benítez, F.L., Rivas-Torres, G., Sampedro, C., Arce-Nazario, J., 2019. Land Cover Classification of Complex Agroecosystems in the Non-Protected Highlands of the Galapagos Islands. Remote Sens. (Basel). 12, 65. https://doi.org/10.3390/rs12010065

Lindsay, J.B., Seibert, J., 2013. Measuring the significance of a divide to local drainage patterns. International Journal of Geographical Information Science 27, 1453–1468. https://doi.org/10.1080/13658816.2012.705289

Martín-Velázquez, S., Rodríguez-Santalla, I., Ropero-Szymañska, N., Gomez-Ortiz, D., Martín-Crespo, T., de Ignacio-San José, C., 2022. Geomorphological Mapping and Erosion of Abandoned Tailings in the Hiendelaencina Mining District (Spain) from Aerial Imagery and LiDAR Data. Remote Sens. (Basel). 14, 4617. https://doi.org/10.3390/rs14184617

Padró, J.-C., Carabassa, V., Balagué, J., Brotons, L., Alcañiz, J.M., Pons, X., 2019a. Monitoring opencast mine restorations using Unmanned Aerial System (UAS) imagery. Science of The Total Environment 657, 1602–1614. https://doi.org/10.1016/j.scitotenv.2018.12.156

Padró, J.-C., Cardozo, J., Montero, P., Ruiz-Carulla, R., Alcañiz, J.M., Serra, D., Carabassa, V., 2022. Drone-Based Identification of Erosive Processes in Open-Pit Mining Restored Areas. Land (Basel). 11, 212. https://doi.org/10.3390/land11020212

Padró, J.-C., Muñoz, F.-J., Planas, J., Pons, X., 2019b. Comparison of four UAV georeferencing methods for environmental monitoring purposes focusing on the combined use with airborne and satellite remote sensing platforms. International Journal of Applied Earth Observation and Geoinformation 75, 130–140. https://doi.org/10.1016/j.jag.2018.10.018

Pell, T., Li, J.Y.Q., Joyce, K.E., 2022. Demystifying the Differences between Structure-from-MotionSoftware Packages for Pre-Processing Drone Data. Drones 6, 24. https://doi.org/10.3390/drones6010024

Pons, X., 2004. Sistema de Información Geográfica y software de Teledetección [WWW Document]. https://www.miramon.cat/help/spa/.

Ren, H., Zhao, Y., Xiao, W., Hu, Z., 2019. A review of UAV monitoring in mining areas: current status and future perspectives. Int. J. Coal Sci. Technol. 6, 320–333. https://doi.org/10.1007/s40789-019-00264-5

Renette, C., Olvmo, M., Thorsson, S., Holmer, B., Reese, H., 2024. Multitemporal UAV lidar detects seasonal heave and subsidence on palsas. Cryosphere 18, 5465–5480. https://doi.org/10.5194/tc-18-5465-2024

Riverscapes Consortium, 2025. GCD [WWW Document]. https://gcd.riverscapes.net/.

Sabzevari, T., Talebi, A., 2019. Effect of hillslope topography on soil erosion and sediment yield using USLE model. Acta Geophysica 67, 1587–1597. https://doi.org/10.1007/s11600-019-00361-8

Sendrós, A., Cubides, I.J., Himi, M., Lovera, R., Urruela, A., Tapias, J.C., Rivero, L., Garcia-Artigas, R., Casas, A., 2023. Coupled Geophysical and Hydrogeochemical Characterization of a Coastal Aquifer as Tool for a More Efficient Management (Torredembarra, Spain). Water (Basel). 15, 3333. https://doi.org/10.3390/w15193333

Solé, P., Ferrer, D., Raya, I., Pous, M., Gonzàlez, R., Marañón-Jiménez, S., Alcañiz, J.M., Carabassa, V., 2023. Physical and Chemical Properties of Limestone Quarry Technosols Used in the Restoration of Mediterranean Habitats. Land (Basel). 12, 1730. https://doi.org/10.3390/land12091730

Wang, Y., Koo, K.-Y., 2021. Vegetation Removal on 3D Point Cloud Reconstruction of Cut-Slopes Using U-Net. Applied Sciences 12, 395. https://doi.org/10.3390/app12010395

Xiao, D., Pan, Y., Feng, J., Yin, J., Liu, Y., He, L., 2022. Remote sensing detection algorithm for apple fire blight based on UAV multispectral image. Comput. Electron. Agric. 199, 107137. https://doi.org/10.1016/j.compag.2022.107137

Xie, J., Liu, X., Bai, P., Liu, C., 2022. Rapid Watershed Delineation Using an Automatic Outlet Relocation Algorithm. Water Resour. Res. 58. https://doi.org/10.1029/2021WR031129

Xinwei, Z., Yunchao, Z., Qiulan, F., 2023. Main influencing factors of soil particle distribution in the karst basin. Catena (Amst). 224, 107002. https://doi.org/10.1016/j.catena.2023.107002